Catalysis Letters 35 (1995) 89–106

A novel method to produce nanocrystalline metastable supported catalysts

R. Schulz [a], A. Van Neste [b], P.A. Zielinski [c], S. Boily [b], F. Czerwinski [d], J. Szpunar [d] and S. Kaliaguine [c]

[a] *Technologie des Matériaux, Institut de Recherche d'Hydro-Québec, 1800 Montée Ste-Julie, Varennes, Québec, Canada J3X 1S1*

[b] *Département de Métallurgie,* [c] *Département de Génie Chimique, Université Laval, Ste-Foy, Québec, Canada G1K 7P4*

[d] *Department of Metallurgical Engineering, McGill University, Montréal, Québec, Canada H3A 2A7*

Received 30 December 1994; accepted 22 June 1995

The high energy ball-milling technique has been used to produce metastable Ni(Ru) alloys supported on alumina. This catalyst has potential application for the hydrogenation of the C=O bond. The active species are first formed by mechanical alloying pure Ni and Ru powders. The alumina support is ground independently until no structural transformation occurs. Finally, the supersaturated Ni(Ru) powder is milled with the alumina support to produce highly dispersed individual Ni(Ru) nanocrystals on the surface of Al_2O_3. This supported catalyst has been characterized by X-ray diffraction, transmission electron microscopy, X-ray photoelectron spectroscopy and thermal desorption spectroscopy.

Keywords: supported catalyst; nanocrystalline alloys; metastable alloys; ball milling; mechanical alloying; surface

1. Introduction

To optimize the properties of a catalyst for a given reaction, one would like to be able to choose the composition and the structure of the active species independently of the limits of the thermodynamics and disperse the particles on a substrate in a way to maximize the effective surface area. The current methods of producing supported catalysts do not allow such a versatility. For instance, if the catalyst is produced by pyrolysis of organometallic compounds [1], the high temperature used in the process limits the range of composition accessible and the dispersion on the surface is controlled by the decomposition/nucleation and growth processes. In recent years, several techniques have been developed to produce alloys with non-equilibrium structure and composition. Crystalline supersaturated solid-solutions [2], amorphous alloys [3] and nanocrystalline materials [4,5] are all new states of

matter, the catalytic properties of which have not been studied thoroughly. High energy ball milling is a simple technique which, recently, has been used quite extensively to produce metastable nanocrystalline alloys with various compositions [6]. The powder particles of the milled product are agglomerates of crystals, the size of which is typically less than a few nanometers. The powder cannot be used as such for catalysis because the effective surface area is too small. This paper describes a method which breaks the powder particles into individual nanocrystals and disperses them on a substrate. The system which has been chosen is Ni(Ru)/Al_2O_3 for potential application as catalyst for the hydrogenation of the C=O bond. Both Ni and Ru are good catalysts for this reaction but, according to Balandin's multiplet theory of catalysis, an optimum in the properties could be reached if the interatomic distance in the catalyst would be 2.58 Å, a value which is between the distance of closest approach in Ni (2.492 Å along [110] in fcc Ni) and Ru (2.65 Å along [423] in hcp Ru) [7]. By ball-milling mixtures of Ni and Ru powders, nanocrystalline supersaturated solid solutions with various lattice parameters can be obtained.

2. Experimental

99.95% pure Ni and Ru elemental powders were obtained from Alfa Products (Johnson Matthey). The particle size was –120 mesh for Ni and –325 mesh for Ru. The γ-alumina powder used for the support is from Norton. The initial surface area is 208.2 m^2/g and the pore volume is 0.557 cm^3/g. A SPEX 8000 instrument was used for milling. A hardened steel vial, three steel balls (11 mm in diameter) and a typical milling charge of 4 g were used for alumina while a tungsten carbide (WC) crucible, three WC balls (11 mm in diameter) and a ball-to-powder weight ratio of 5 to 1 were used for Ni–Ru. The crucibles were kept hermetically sealed with a viton O-ring during milling. For alumina, the loading of the powder and all subsequent samplings were performed in air while for Ni–Ru and Ni(Ru) with alumina, the powder handling was done in a glove box under an argon atmosphere.

The X-ray diffraction patterns were taken with a Philips diffractometer using Mo Kα radiation or with a Siemens diffractometer using Cu Kα. The transmission electron micrographs were obtained on a Hitachi H-9000 at 300 kV. The instrument is equipped with a low-Z energy dispersive X-ray (EDX) detector from Link. The samples for TEM were prepared by, first, dispersing the powder in ethanol using an ultrasonic bath, then depositing a drop of liquid containing the particles in suspension on a TEM grid coated with amorphous carbon or SiO_2. The particle size distribution of the active species was evaluated using TEM bright field images and a Tracor Northern TN-8500 image analyzer. The X-ray photoelectron spectroscopy was performed with a Perkin Elmer Phi-5500. The spectra were measured with an Al Kα monochromatic source and were referenced to the C 1s peak at 284.8 eV. Surface areas were measured by the Brunauer, Emmett and Teller method (BET) using a computer-controlled sorption analyzer (Omnisorp 100). Samples of 0.1 g

were heated under vacuum at 300°C for 1 h prior to the adsorption–desorption experiments. Temperature programmed desorption (TPD) experiments were carried out using an Altimira apparatus. The samples were pretreated at 300°C for 1 h in flowing hydrogen then cooled to room temperature for hydrogen adsorption. The chamber is flushed with argon for half of an hour before the desorption experiment. The argon flow rate is 30 cm^3/min and the heating rate is 15°C/min from room temperature to 600°C. The thermal stability of the metastable alloys was investigated using a differential thermal analyzer from Perking Elmer.

3. Results and discussion

3.1. THE ACTIVE PARTICLES

In thermodynamic equilibrium, the solubility of Ru in fcc Ni at room temperature is less than 4 at% [8]. By mechanical alloying, it has been possible to produce supersaturated fcc Ni(Ru) solid solutions up to a Ru content of about 38 at% [9]. Fig. 1 shows the evolution of the X-ray spectrum of a mixture of Ni and Ru powders as a function of milling time for a composition $Ni_{65}Ru_{35}$. During milling, Ru diffuses into the fcc structure. The X-ray peaks of Ru disappear gradually while the

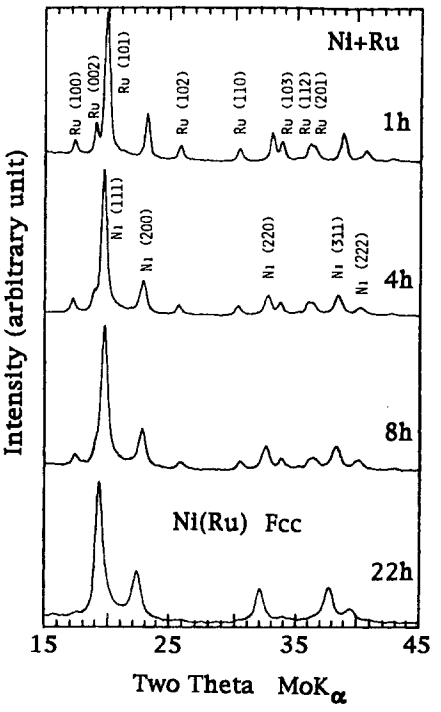

Fig. 1. X-ray diffraction patterns of a mixture of Ni and Ru powders of composition $Ni_{65}Ru_{35}$ as a function of milling time.

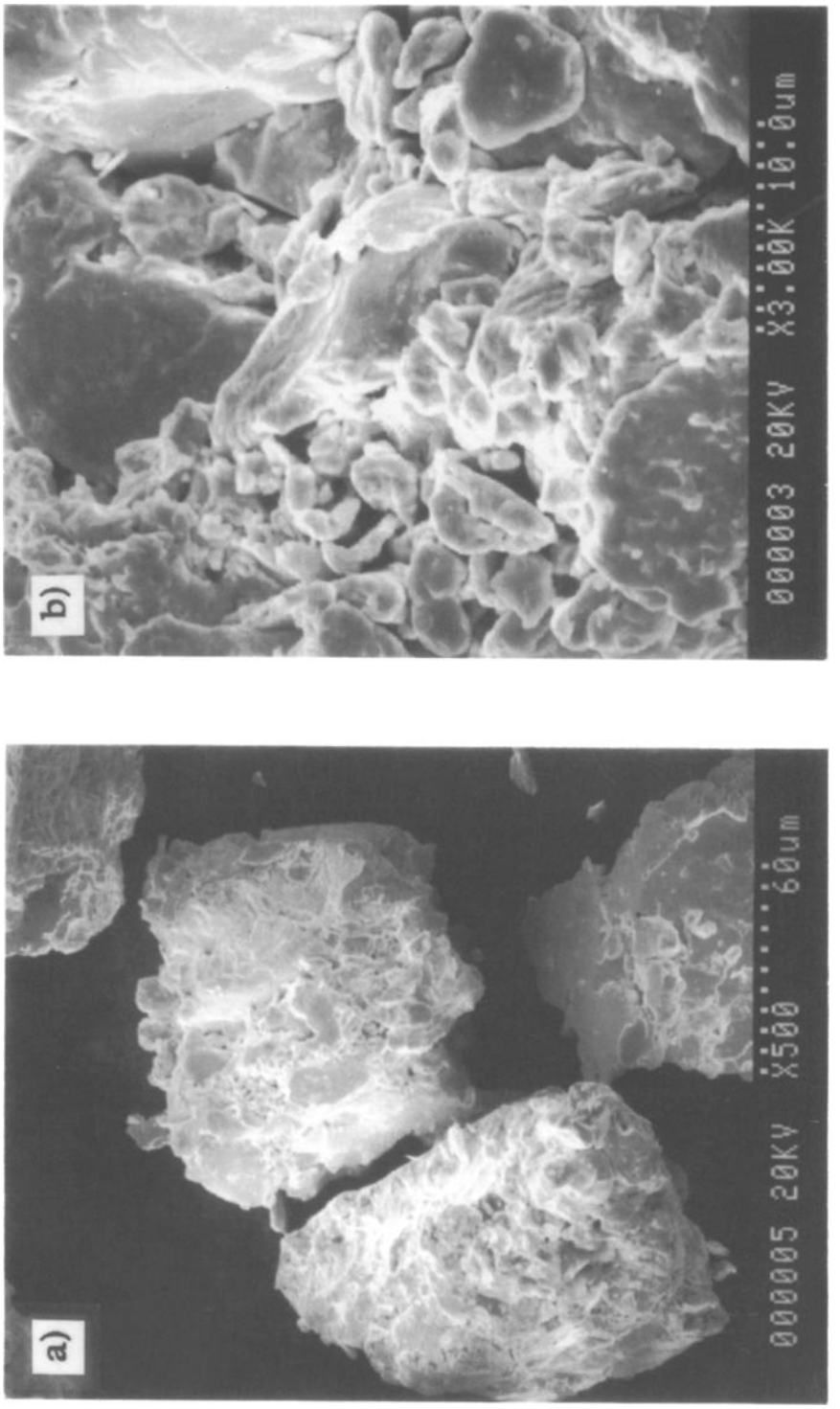

Fig. 2. Scanning electron micrographs of Ni(Ru) powders after 22 h of milling.

peaks of Ni shift toward the low angles because of the expansion of the unit cell. After 22 h, the structure is almost fcc single phase. The distance of closest approach between the atoms in the structure is 2.56 Å, a value which is close to the optimum distance according to Balandin's model. Using the Scherrer formula and the width at half maximum of the main diffraction peak, an average crystal size of about 6 nm was estimated. The size of the powder particles ranges from a few microns to about 100 μm (fig. 2) and, according to the BET technique, the surface area is less than 1 m^2/g. This is much too small to be of interest for catalysis.

3.2. THE ALUMINA SUPPORT

There are seven known phases of alumina. All are metastable except the α-phase which can be obtained from the other phases by high temperature heat treatment at about 1200°C. Since high temperatures are required to synthesize the α-phase, its specific surface area is quite small (0.1–5 m^2/g) [10]. This keeps it from being a useful support for catalysis. Therefore, a metastable γ-alumina powder with an initial surface area of 208 m^2/g was chosen for the present work.

The γ-alumina was milled in a hardened steel crucible in air until no structural change is observed. Fig. 3 shows the X-ray patterns as a function of milling time. The initial fcc structure is shown at the bottom. The width of the peaks suggests that the initial crystal size is quite small. One can distinguish two relatively high maxima. The (400) line at $2\theta = 45.91°$ and the (440) at $2\theta = 66.9°$. One can easily see that the (400) reflection which only belongs to the γ-phase decreases in intensity and vanishes almost completely after 12 h of milling while the (440) line splits in two peaks. The structure changes from fcc to hcp. After 12 h, the powder has the structure of the α-phase. The top spectrum shows the X-ray diffraction pattern of pure α-alumina (Johnson Matthey 99.99%) for reference. Therefore, it is possible to produce, at room temperature, the α-phase by simple mechanical deformation of γ-alumina. This is also true for several other transition aluminas [11].

The specific surface area decreases by about a factor of two during the milling process. Fig. 4a shows that most of the changes occur during the first 3–4 h of milling. If the process is performed in a sealed crucible under argon instead of air, the final surface area is much lower [11]. This indicates that the supply of oxygen is necessary to saturate the broken bonds on fresh fractured surfaces and prevent the agglomeration of particles.

The pore size distribution changes also significantly during the milling process as shown in fig. 4b. The total pore volume decreases from 0.557 cm^3/g to 0.138 cm^3/g after 6 h of milling. Initially, most of the pores have a radius between 3 and 4 nm. After milling, the distribution follows a monotonic decrease with the maximum located between 1 and 2 nm.

Although large changes are observed in the structure and morphology of the alumina powder, the material remains, after milling, interesting for catalysis since the final specific surface area is still quite high.

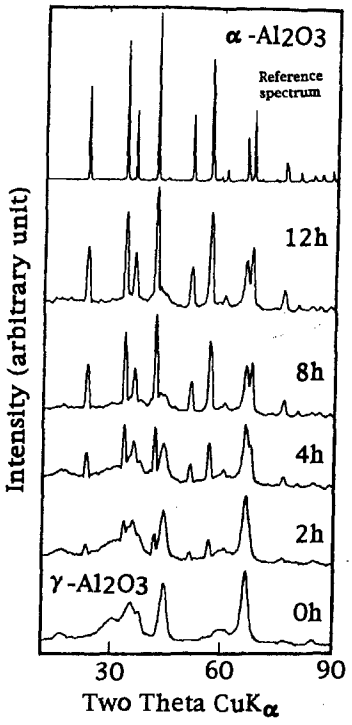

Fig. 3. X-ray diffraction patterns of γ-alumina as a function of milling time. The top spectrum of α-alumina is shown for comparison.

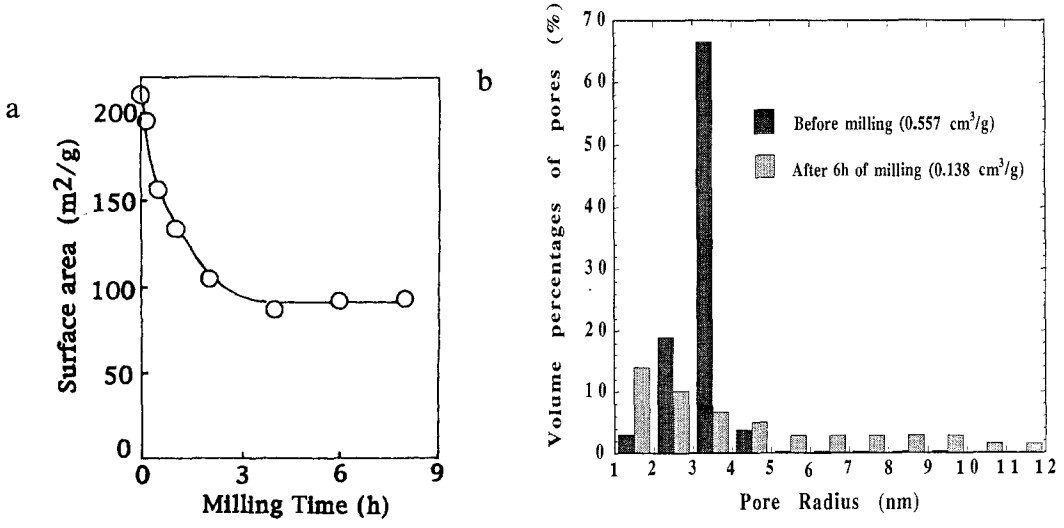

Fig. 4. (a) The specific surface area of the alumina powder as a function of the milling time in air and using steel vial. (b) Pore size distribution before and after 6 h of milling in air.

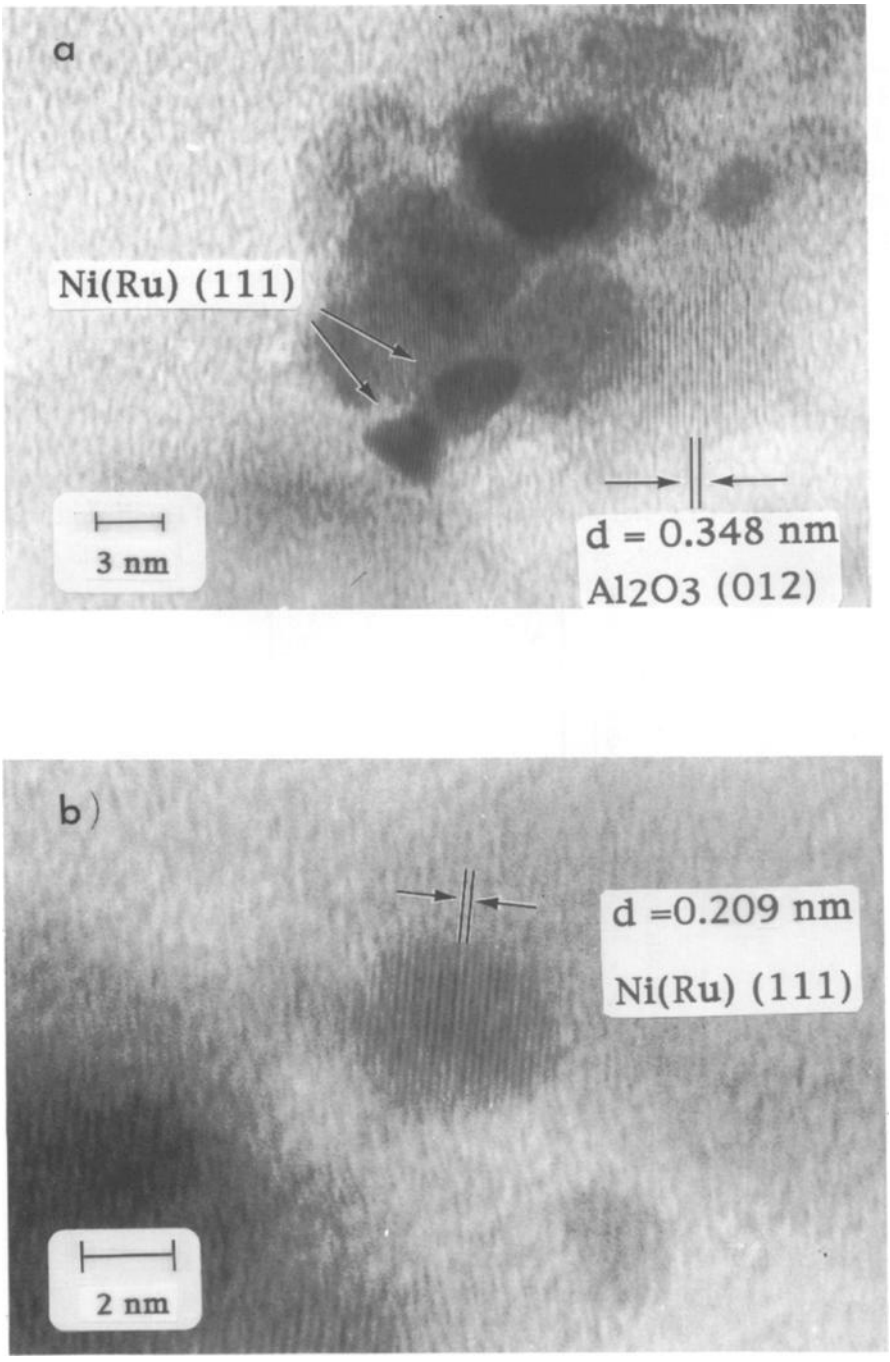

Fig. 5. High resolution TEM micrographs of Ni(Ru)/Al_2O_3 after 48 h of milling with the alumina support.

3.3. DISPERSION OF THE ACTIVE PARTICLES BY ALUMINA

The supported catalyst was prepared by milling, under argon, the supersaturated $Ni_{65}Ru_{35}$ (22 h milled) alloy in a WC crucible with α-alumina obtained from pre-milled γ-alumina. A mixture with 20 wt% of metallic particles was used. The milling process breaks the large metallic agglomerates into small nanocrystalline particles and disperses them on the alumina support.

Figs. 5a and 5b show, after 48 h of milling, high resolution TEM micrographs of fcc Ni(Ru) particles on the alumina support. One can distinguish, in fig. 5a, the (111) lattice fringes of Ni(Ru) with a d spacing of 0.209 nm. The (012) lattice fringes of Al_2O_3 with $d = 0.348$ nm are also visible. Fig. 5b shows a single nanocrystal on the alumina support. The diameter of the particle is between 3 and 4 nm, a value which is slightly lower than the average $Ni_{65}Ru_{35}$ crystal size before milling with the alumina.

Fig. 6 shows EDX spectra taken (a) on the alumina support and (b) at the center of the particle shown in fig. 5b. These chemical analyses confirm the nature of the

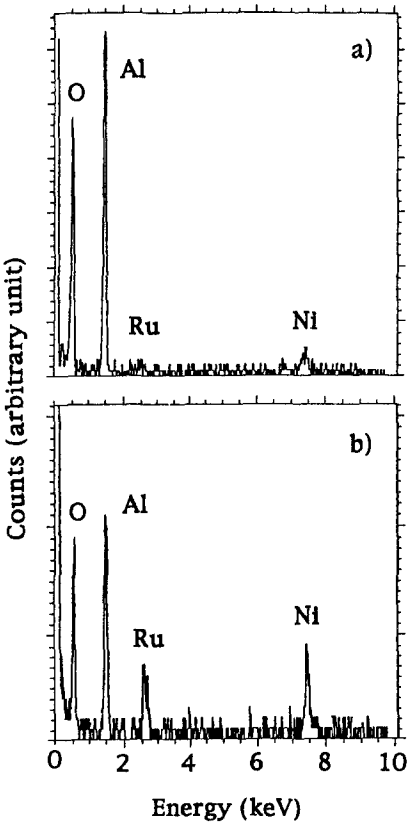

Fig. 6. Energy dispersive X-ray spectra of (a) the alumina support and (b) the Ni(Ru) particle shown in fig. 5b.

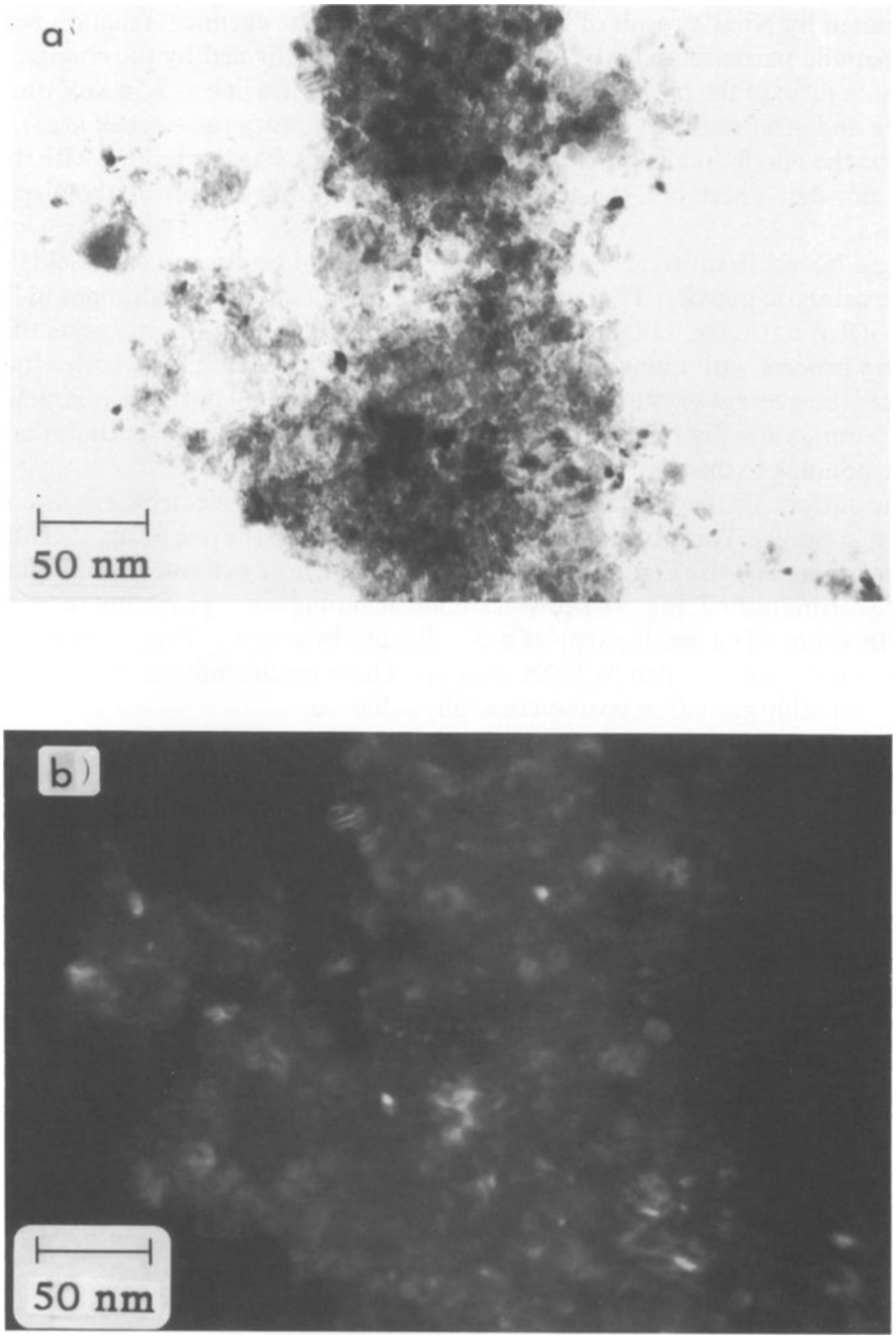

Fig. 7. Low resolution TEM bright (a) and dark (b) field micrographs of Ni(Ru)/Al_2O_3 catalyst after 48 h of milling with alumina.

particles found on the alumina support and suggest that Al_2O_3 may have been contaminated by Ni as a result of the milling process. The chemical reaction between the metallic particles and Al_2O_3 during milling is confirmed by the change in the intensity ratio of the Ni Kα peak at 7.47 keV and Ru Lα line at 2.56 keV observed before and after milling with Al_2O_3. The Ni/Ru intensity ratio (peak area) measured on the $Ni_{65}Ru_{35}$ alloy is close to 3 while it is near 1.75 after milling with the alumina powder. Therefore, the active particles loose some Ni during the dispersion process.

Figs. 7a and 7b show, at lower magnification, TEM bright and dark field images of the catalytic powder. The dark particles in fig. 7a and the bright ones in fig. 7b are Ni(Ru) particles. Lots of them are smaller than 5 nm. This suggests that the milling process with alumina not only breaks the metallic agglomerates but also reduces the average crystal size. Fig. 8 shows, for the small particles (diameter less than 5 nm), a size distribution obtained from fig. 7a. The average particle diameter corresponding to this distribution is 2.5 nm.

The surface of the powder, as observed on a scanning electron microscope, is shown in fig. 9a. The morphology is very different from the one of fig. 2. There are grains of various sizes on which a very large number of extremely small particles can be distinguished. Fig. 9b shows a similar scanning micrograph but in transmission this time. The small particles are indicated by arrows. They are the Ni(Ru) active particles as verified by EDX analysis. These results indicate that the dispersion of metallic grains has been successfully achieved.

Hydrogen TPD spectra of a 20 wt% mixture of $Ni_{65}Ru_{35}$ with α-Al_2O_3 ball milled for various times are shown in fig. 10. The top spectrum is from the pure Ni(Ru) powder. The total mass of the metallic component is the same in each spectrum but

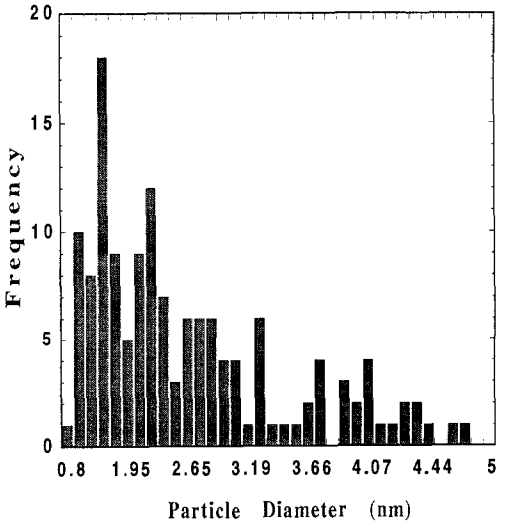

Fig. 8. Ni(Ru) particle size distribution obtained from fig. 7a.

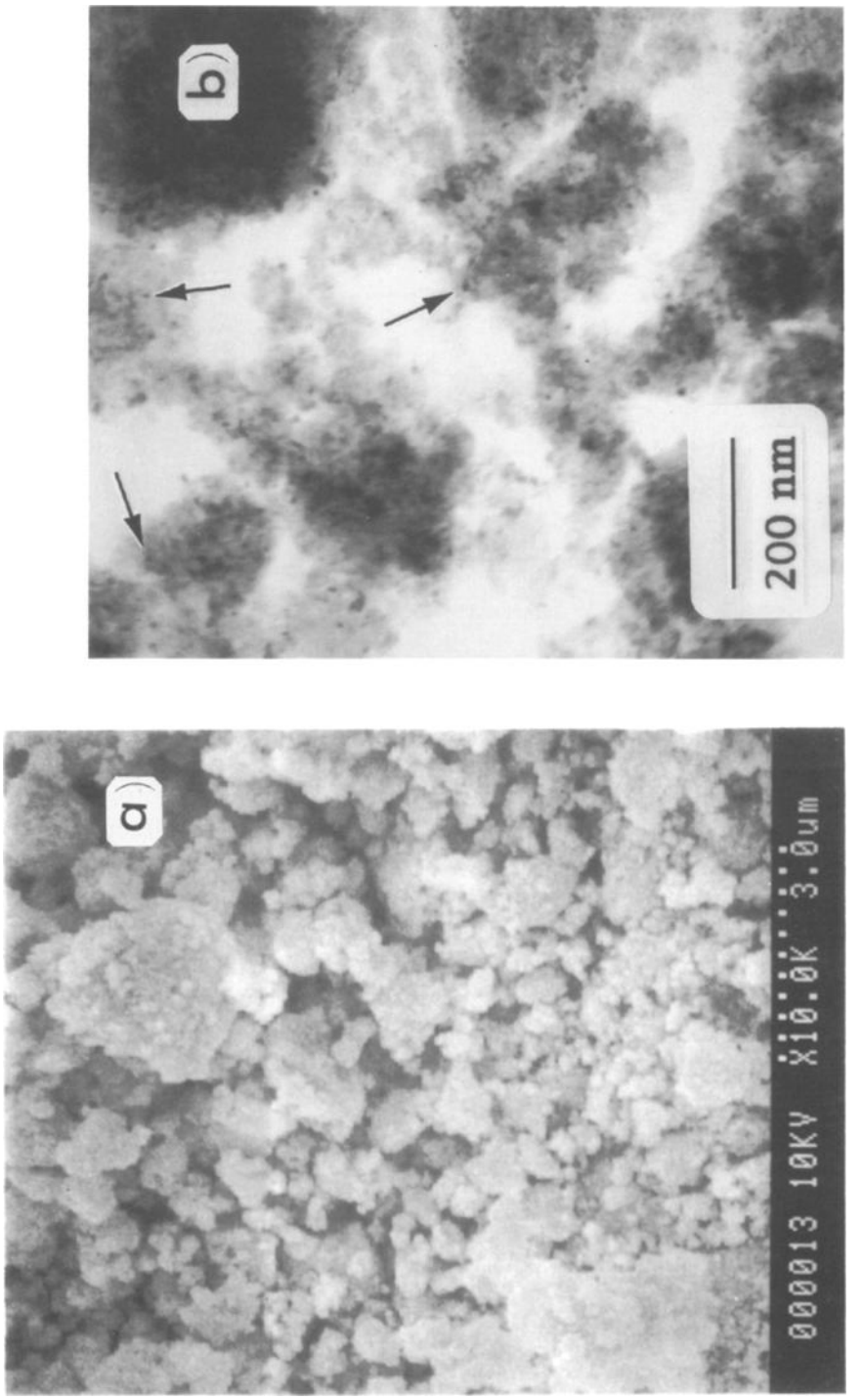

Fig. 9. Scanning reflection (a) and transmission (b) micrographs of the Ni(Ru)/Al_2O_3 catalyst.

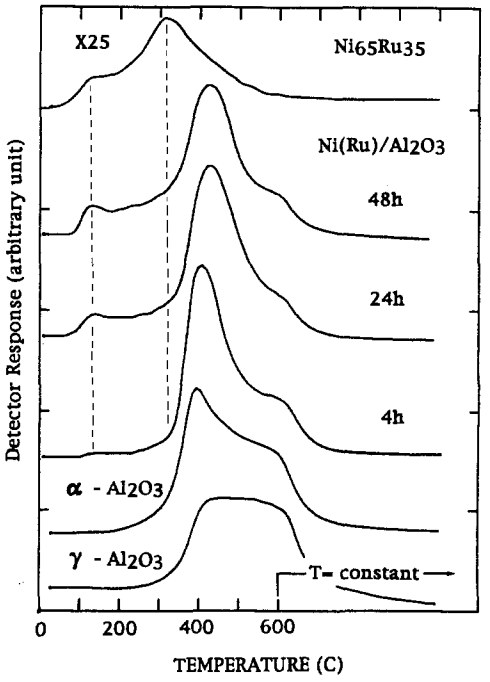

Fig. 10. Temperature programmed desorption (TPD) curves on γ- and α-alumina, Ni(Ru) alloy and Ni(Ru)/Al_2O_3 after various milling times.

the desorption curve of the Ni(Ru) alloy has been multiplied by 25 for visibility. The bottom traces from pure α- and γ-aluminas are also shown for reference.

For the metallic alloy, the spectrum shows two weak maxima at about 100 and 300°C. Similar measurements (not reported here) made on pure Ni and Ru powders show even smaller desorption curves. Two maxima from Ni(111) surfaces were reported at 73 and 111°C [12]. Adsorption on 15 wt% Ni/Al_2O_3 supported catalyst produces one sharp peak below 100°C and a broad high temperature part which depends on the degree of activation [13]. Another report on Ni supported catalysts showed one or two overlapping peaks between 80 and 170°C [14]. For Ru/Al_2O_3 catalysts, two peaks were observed at 175 and 293°C [12]. From these results, one may be tempted to assign the low temperature peak in the TPD spectrum of Ni(Ru) to Ni and the high temperature one to Ru. However, this assignment has to be taken with caution since these metals are alloyed in the present case.

The TPD spectra of Ni(Ru)/Al_2O_3 show a large peak between 300 and 600°C which is attributed to the alumina support and small peaks at low temperature which coincide with those of Ni(Ru). The intensity of the low temperature peaks increases with increasing milling time. This indicates that the specific surface area of the metallic component increases noticeably as a result of the dispersion of the Ni(Ru) alloy. The fact that the low temperature peaks do not shift in temperature

during the milling also indicates that the Ni(Ru) alloy does not change significantly in nature during the process.

The TPD experiments together with the previous microstructural analysis confirm that metastable supported catalysts with large specific surface areas can be produced by high energy ball milling.

X-ray photoelectron spectroscopy (XPS) of the samples before and after milling with the alumina support was also performed. Fig. 11 shows the spectra for the $Ni_{65}Ru_{35}$ metastable supersaturated solid solution before milling with the alumina support and table 1 gives the position and the full width at half maximum (FWHM) of the various peaks. The deconvolution of the spectra was done using Gaussian–Lorentzian peaks. After milling, the alloy was only exposed to the air for a few seconds before being introduced in the spectrometer. The spectra were obtained without sputter cleaning. Fig. 11a shows the Ru peaks. Three phases were

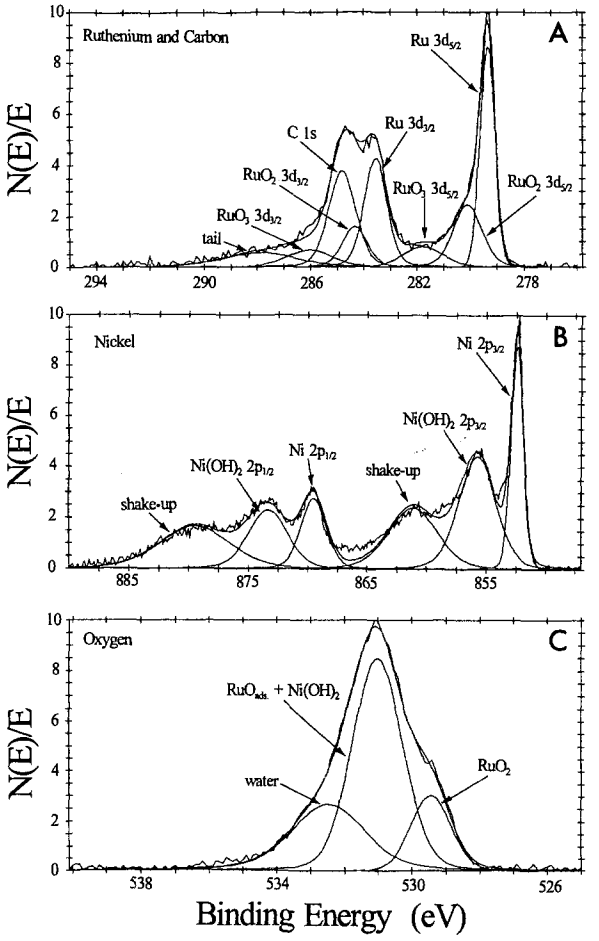

Fig. 11. XPS spectra of $Ni_{65}Ru_{35}$ fcc solid solution.

Table 1
Binding energies and full width at half maximum (FWHM) of the $Ni_{65}Ru_{35}$ alloy

Component	Level	Binding energy (eV)	FWHM (eV)
ruthenium and carbon			
Ru	$3d_{5/2}$	279.36	0.65
RuO_2	$3d_{5/2}$	280.10	1.25
RuO_3	$3d_{5/2}$	281.77	1.80
Ru	$3d_{3/2}$	283.55	1.00
RuO_2	$3d_{3/2}$	284.33	1.10
C	1s	284.80	1.20
RuO_3	$3d_{3/2}$	286.02	2.00
tail	–	287.91	3.30
nickel			
Ni	$2p_{3/2}$	852.39	1.22
$Ni(OH)_2$	$2p_{3/2}$	855.72	3.65
shake-up	–	861.13	4.90
Ni	$2p_{1/2}$	869.51	2.50
$Ni(OH)_2$	$2p_{1/2}$	873.35	3.89
shake-up	–	879.46	6.90
oxygen			
RuO_2	1s	529.43	1.40
$RuO_{ads} + Ni(OH)_2$	1s	531.01	1.77
water	1s	532.47	2.60

identified: metallic Ru, RuO_2 and RuO_3. The C 1s peak at 284.80 eV falls between the RuO_2 and RuO_3 $3d_{3/2}$ levels. The peak positions, the energy differences and intensity ratios of the $3d_{5/2}$ and $3d_{3/2}$ peaks agree well with previously reported values [15]. Fig. 11b shows the Ni peaks. Best fits were obtained using two phases, metallic Ni and $Ni(OH)_2$ [16,17]. Fig. 11c confirms that oxygen is found primarily in the form of $Ni(OH)_2$ and RuO_2. However, the peak at 531.01 eV could also correspond to chemisorbed atomic oxygen on Ru [15]. Oxygen in water appears at 532.47 eV.

A similar XPS study on the Ni–Ru catalyst after milling with the alumina support has also been performed. In the as-prepared condition, the Ru and Ni metallic peaks are not visible. However, by ion bombardment with Ar^+ ions, the metallic components are revealed. The spectra, after few minutes of sputtering, are shown in fig. 12. They are quite similar to the ones of fig. 11. The various phases are still Ru, RuO_2, RuO_3, Ni and $Ni(OH)_2$. The binding energies shown in table 2 for the alumina supported catalyst are almost identical to the ones found in table 1 suggesting very little chemical interaction between the catalytic species and the alumina support. Moreover, the Ni/Ru concentration ratio measured by XPS stays practically constant during the milling with alumina indicating that there is no preferential loss of Ni or Ru from the powder surface. This concentration ratio equals

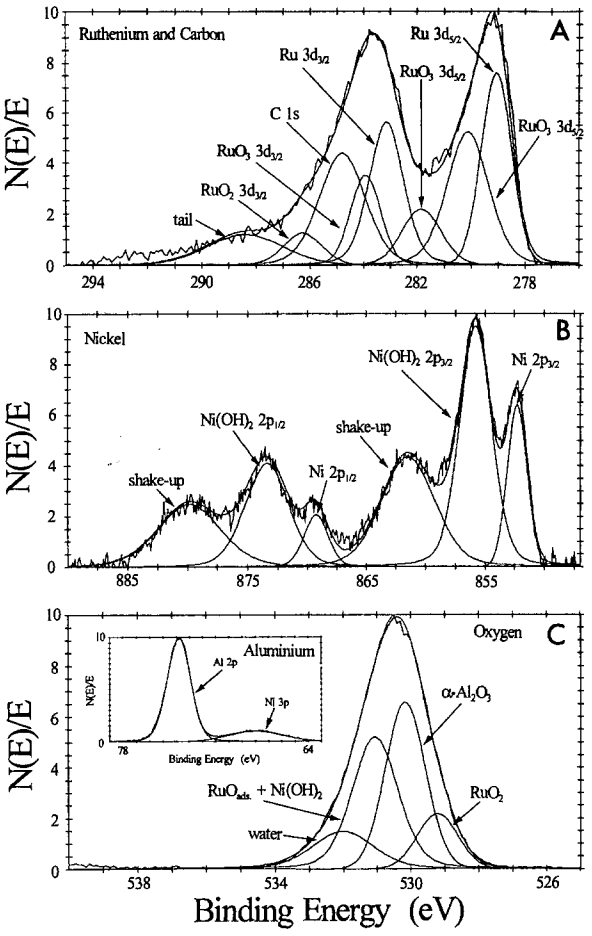

Fig. 12. XPS spectra of $Ni_{65}Ru_{35}$ supported on α-Al_2O_3.

1.824 as expected from the initial alloy composition. The oxygen peak, however, (fig. 12c), differs from the previous one by the fact that it has an additional component located at 530.15 eV: the oxygen in α-Al_2O_3. The corresponding Al 2p level, shown in the inset of fig. 12c, is located at 73.80 eV in agreement with reported values for α-Al_2O_3 [18]. The intensity ratios between the α-Al_2O_3 peak and the peaks of $Ni(OH)_2 + RuO_{ads}$ and RuO_2 indicate a good dispersion of the catalytic species.

In order to be useful catalysts for the hydrogenation of the C=O bond, these metastable nanocrystalline supersaturated solid solutions have to be thermally stable at the operating temperature of chemical reactors. The typical operating temperatures for those reactions are usually between 180 and 300°C. The DTA (differential thermal analysis) traces shown in fig. 13 for two metastable nanocrystalline alloys indicate that the metastable fcc Ni(Ru) alloy is stable up to about 400°C

Table 2
Binding energies and full width at half maximum (FWHM) of the $Ni_{65}Ru_{35}$ alloy supported on α-alumina

Component	Level	Binding energy (eV)	FWHM (eV)
ruthenium and carbon			
Ru	$3d_{5/2}$	279.07	1.30
RuO_2	$3d_{5/2}$	280.13	1.80
RuO_3	$3d_{5/2}$	281.84	1.70
Ru	$3d_{3/2}$	283.15	1.50
RuO_2	$3d_{3/2}$	284.93	1.31
C	1s	284.80	2.00
RuO_3	$3d_{3/2}$	286.28	1.70
tail	–	288.39	3.30
nickel			
Ni	$2p_{3/2}$	852.29	1.98
$Ni(OH)_2$	$2p_{3/2}$	855.80	3.20
shake-up	–	861.49	5.30
Ni	$2p_{1/2}$	869.27	2.35
$Ni(OH)_2$	$2p_{1/2}$	873.39	4.24
shake-up	–	879.85	6.20
oxygen			
RuO_2	1s	529.20	1.40
α-Al_2O_3	1s	530.15	1.40
RuO_{ads} + $Ni(OH)_2$	1s	531.05	1.60
water	1s	532.00	2.13
aluminium			
Al	2p	73.80	2.05

after which thermal decomposition occurs. The supersaturated hcp Ru(Ni) alloy is slightly more stable, the onset of thermal decomposition being 500°C.

4. Conclusions

A method of synthesizing metastable supported catalysts has been demonstrated. The method consists of three parts. In a first step, the metastable catalytic species are fabricated by high energy mechanical alloying. Non-equilibrium alloys (Ni–Ru in the present case) in the form of powder and with various compositions can thus be formed. In a second step, the support (high specific surface area alumina in this case) is milled independently until no structural changes are observed. In a final step, the catalytic powder is milled with the alumina to break the particles into individual Ni(Ru) nanocrystals which are dispersed on the alumina support.

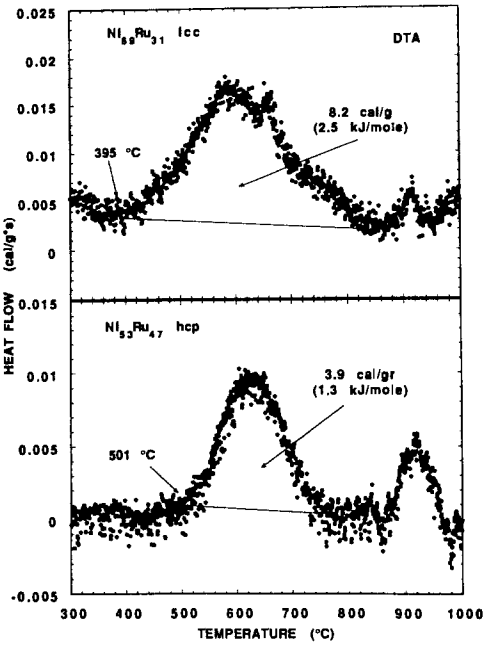

Fig. 13. DTA traces of a nanocrystalline metastable $Ni_{69}Ru_{31}$ fcc solid solution and of a $Ni_{53}Ru_{47}$ hcp alloy.

Very little chemical interaction is observed between the catalytic species and the alumina during this process. The specific surface area of the metallic active component increases significantly. This method offers the possibility of producing novel supported catalysts of various compositions which would otherwise not be possible to make by conventional techniques.

Acknowledgement

The authors would like to thank Rene Dubuc, Alain Joly, Reynald Rioux and Michel Trudeau for technical assistance.

References

[1] M. Ladouceur, G. Lalande, D. Guay, J.P. Dodelet, L. Dignard-Bailey, M.L. Trudeau and R. Schulz, J. Electrochem. Soc. 140 (1993) 1974.
[2] A.W. Weeber and H. Bakker, Physica B 153 (1988) 93.
[3] M. Trudeau, J.Y. Huot and R. Schulz, J. Appl. Phys. 67 (1990) 2333.
[4] J.Y. Huot, M. Trudeau and R. Schulz, J. Electrochem. Soc. 138 (1991) 1316.
[5] M.L. Trudeau, J.Y. Huot and R. Schulz, Appl. Phys. Lett. 58 (1991) 2764.

[6] A. Van Neste, S. Kaliaguine, M. Trudeau and R. Schulz, Materials Research Society Symp. Proc. 205 (1992) 227.
[7] N.A. Vasyunina, G.S. Barysheva and A.A. Balandin, Izv. Akad. Nauk SSSR, Ser. Khim. 4 (1969) 848.
[8] Hansen, *Constitution of Binary Alloys*, 2nd Ed. (McGraw-Hill, New York, 1985).
[9] A. Van Neste, A. Lamarre, M.L. Trudeau and R. Schulz, J. Mater. Res. 7 (1992) 2412.
[10] J.R. Anderson, *Structure of Metallic Catalysts* (Academic Press, London, 1975).
[11] P.A. Zielinski, R. Schulz, S. Kaliaguine and A. Van Neste, J. Mater. Res. 8 (1993) 2985.
[12] K.D. Rendulic, A. Winkler and H.P. Steinruck, Surf. Sci. 185 (1987) 469.
[13] T. Paryjczak and E. Lesniewska, React. Kinet. Catal. Lett. 33 (1987) 203.
[14] Altamira Notes, *Development of a Quality Control Procedure for Characterizing Supported Ni Catalysts*, March 1992.
[15] K.S. Kim and N. Winograd, J. Catal. 35 (1974) 66.
[16] N.S. McIntyre and M.G. Cook, Anal. Chem. 47 (1975) 2208.
[17] D.B. Mitton, J. Walton and G.E. Thompson, Surf. Inter. Anal. 20 (1993) 36.
[18] J.F. Moulder, W.F. Stickle, P.E. Sobol and K.D. Bomben, *Handbook of X-ray Photoelectron Spectroscopy* (Perkin Elmer).